Analysis on Dust Devil Containing Loess Dusts of Different Sizes

Z.L. Gu[1*], J. Qiu[2], Y.Z. Zhao[3], X.P. Hou[2]

[1] *Department of Environmental Science and Technology, School of Human Settlements and Civil Engineering, Xi'an Jiaotong University, Xi'an 710049, P.R. China*

[2] *School of Energy and Power Engineering, Xi'an Jiaotong University, Xi'an 710049*

[3] *Department of Chemical Engineering, Tsinghua University, Beijing 100084, P.R. China*

Abstract

Dust devil in convective boundary layer (CBL) was simulated by Euler-Lagrange approach. By means of large-eddy simulation method and smoothly stretched grid, flow fields of the small scale whirlwind were obtained. Movements of 20,000 dust particles were tracked by computing external forces and velocities with the aid of the simulated high-resolution air flow fields. Characteristics of the simulated airflow were in good accordance with field observations. Distribution of particles reproduced the shape of dust devil. Statistics of particle trajectories revealed basic properties of the movement of dust particles. Small particles with diameter of 0.04 mm were able to form a rolling cylinder and to be lifted easily to a certain height. 0.1 mm dust particles spiraled upwards like a cone with a small cone angle. Particles with diameters of 0.16 mm and 0.3 mm were obviously thrown outward with limited lifting height and fell back to the ground. The negative vertical pressure gradient in the dust devil strengthened particle lifting, unlike in the horizontal wind systems where the vertical pressure gradient isn't the major driving force. Numerical results showed why total suspended particulates (TSP) concentration exceeded the standard value greatly all the year round on the Loess Plateau, where the loess dust from the local ground was one of the major sources of air pollutants. 90% loess dusts were smaller than 0.04 mm in diameter, which made them easily lifted to a high altitude by dust devils even without obvious horizontal wind. Because thermal plumes are common in CBL, dust devils can occur frequently in multi-locations of the Loess Plateau. According to nature circumstances of the Loess Plateau and thermodynamic characteristics of dust devil, the dust-devil-scale simulation indicated one source of the background TSP on the Loess Plateau and how they were lifted into the atmosphere.

***Keywords*:** Dust devil; Gas-particle flow; Convective boundary layer; Model simulation; Particle size.

* Corresponding author. Tel.: +86-29-82665111

E-*mail address*: *guzhaoln@mail.xjtu.edu.cn*

INTRODUCTION

A small whirlwind in the convective boundary layer (CBL) occurring in sand-rich areas can lift small particles and form visible dust column, or the so-called dust devil, as shown in Fig. 1. Recent researches and evidences have manifested that dust devil is a universal dust transport system (Metzger, 1999; Leovy, 2003; Gu *et al.*, 2006). Vertical vortex of air comes into being when hot air near the ground rises, the vorticity makes the nearby air inflow spiral to the low pressure center under the thermal (Smith and Leslie, 1976; Renno *et al.*, 1998; Kanak *et al.*, 2000), and the fast spinning air can be strong enough to lift dust and sand as shown in Fig. 2. It is observed that temperature raises 4-8 K, and pressure drops 2.5-4.5 hPa in the core of the dust devil as compared with ambient air (Ives, 1947; Sinclair, 1973; Hess and Spillane, 1990; Xu, 2002). Both vertical and tangential velocities can reach 15 m/s. The dimension of the visible dust devil column varies with the whirlwind. Sinclair (1973) reported that the dimension was tens of meters in diameter and 600 meters in height in the deserts of Arizona. Hess and Spillane (1990) observed dust columns of 32-141 m in diameter and 300-600 m in height in Australia. Most dust devils last only a few minutes, traveling with the wind. Therefore, single dust devil is definitely a micro-meteorological phenomenon, and many aspects of dust devils (including the inner structure, the environmental impacts, and the detailed picture of dust devil evolution, etc) were at large obscured. Preliminary estimation of the weight of dust-devil-lifted dust/sand (Hall, 1981; Metzger, 1999) showed that the contribution of dust devils to floating dusts is about one magnitude larger than vehicles in arid lands. Greeley *et al.* (2003) and Gu *et al.* (2006) had discussed particle threshold of dust lifting in dust devils. These studies pointed out the importance of detailed researches on dust devils which would benefit evaluating the total impacts of dust devils on environment.

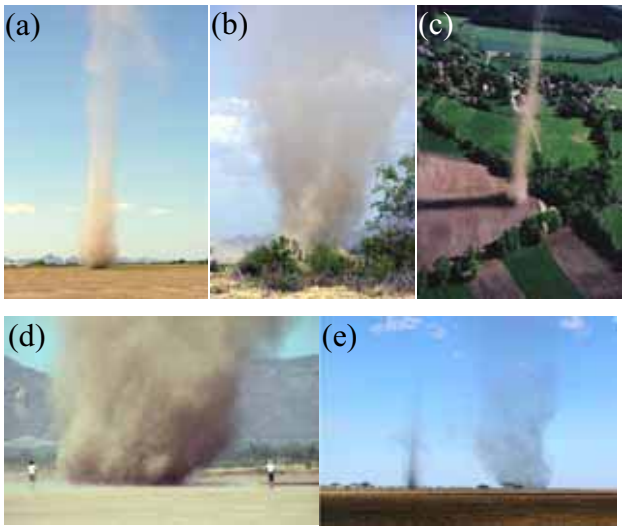

Fig. 1. Photos of dust devils.

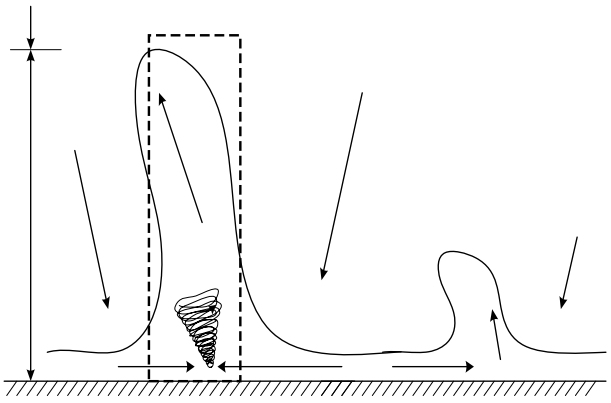

Fig. 2. Sketch of thermal plumes and dust devil in the convective boundary layer.

Dust lifted by dust devils is believed to be one of the major sources of total suspended

particulates (TSP) in arid land where is rich in dust/sand. Take the Loess Plateau for example, even with a low speed of horizontal wind, TSP concentration often exceeds the standard value significantly. How are dusts lifted so as to result in the strong background TSP? Horizontal wind-blown sand system lacks cogent evidences for explanation of the high background TSP. Zhao *et al.* (2004) and Gu *et al.* (2006) provided detailed structure of dust devils and the basic characteristics of dust movements in dust devils by large eddy simulation (LES) approach. Hence, their results showed the way how dust can be easily lifted by dust devils without the presence of strong mean horizontal wind. The area of thermal plumes is about 42% of CBL. The small-scale whirlwind under thermal plume in the right place can bring dusts into the air. Although single dust devil has limited dust lifting capacity, small-scale whirlwinds frequently generated make dust devils occur repeatedly in CBL in arid lands and thus a large amount of dusts are lifted from the ground.

Although the dust devil is commonly observed, simulation of it was notoriously difficult. Gierasch and Goody (1973) proposed a model for Martian dust storm which was also helpful to the simulation of dust devil on earth. Toigo (2003) and Zhao *et al.* (2004), respectively, simulated air flow fields which could result in dust devils. By virtue of the high-resolution simulation, Gu *et al.* (2006) tracked dust grains with different densities and diameters. Numerical simulation of this gas-solid two phase flow gave an insight into the appearance and nature of dust devils. In the present dust-devil-scale simulation, we compared the different shapes of dust devils containing loess dusts with different particle sizes and particle-velocities on the basis of Gu *et al.* (2006). Mathematical models and implementation were given in Section 2, and numerical results and relative discussions were presented in Section 3, and we ended with a summary in Section 4.

MATHEMATICAL MODELS AND IMPLEMENTATION

LES model for the gas phase

Three dimensional LES governing equations for incompressible air are

$$\frac{\partial \overline{u}_i}{\partial x_i} = 0 \tag{1}$$

$$\frac{\partial \overline{u}_i}{\partial t} + \frac{\partial}{\partial x_j}(\overline{u}_i \overline{u}_j) + \frac{1}{\rho_c}\frac{\partial \overline{p}}{\partial x_i} = \frac{\partial \tau_{ij}}{\partial x_j} + g\beta(\overline{T} - T_c)\delta_{i3} \tag{2}$$

$$\frac{\partial \overline{e}}{\partial t} + \frac{\partial (\overline{u}_j \overline{e})}{\partial x_j} = \frac{\partial \zeta_j}{\partial x_j} \tag{3}$$

where the overbar denotes filtering, u_i is velocity component in i direction in Cartesian coordinates, p pressure, e inner energy, t time, T temperature, ρ_c reference density, T_c buoyancy reference temperature, β thermal expansion coefficient, δ_{ij} Kronecker delta. Subgrid-scale (SGS) motions, i.e. turbulent eddies smaller than the filter width, are

parameterized via Germano's dynamic model (Germano *et al.*, 1991). In the Germano's model, the SGS viscosity ν_{SGS}, together with molecular viscosity ν, affects the flow field through the following two SGS terms

$$\tau_{ij} = (\nu + \nu_{SGS})\left(\frac{\partial \overline{u}_i}{\partial x_j} + \frac{\partial \overline{u}_j}{\partial x_i}\right) - \frac{1}{3}\tau_{kk}\delta_{ij} \tag{4}$$

$$\zeta_j = \left(\frac{\nu}{\mathrm{Pr}} + \frac{\nu_{SGS}}{\mathrm{Pr}_{SGS}}\right)\frac{\partial \overline{e}}{\partial x_j} \tag{5}$$

where Pr is Prandtl number, ν is molecular viscosity, SGS Prandtl number $\mathrm{Pr_{SGS}}$ is 0.33, and the SGS viscosity ν_{SGS} is calculated by Germano's dynamic model.

Dust movement model for the particle phase

Dust movement is tracked using the Lagrange approach. Dust particle, the dispersed phase, is assumed to be spherical. Trajectory of each particle is determined by Newton Second Law as

$$m\frac{\mathrm{d}\mathbf{u}_s}{\mathrm{d}t} = \mathbf{F} \tag{6}$$

where m is particulate mass, $\mathbf{u}_s$ particulate velocity vector, $\mathbf{F}$ overall external forces acting on particle (Fan and Zhu, 1998). Main external forces considered in the present study are the drag force, the gravity and the buoyancy force, the pressure gradient force, and the added mass force.

The drag force can be calculated in the form of

$$\mathbf{F}_D = \frac{1}{8}\pi d^2 \rho C_D \,|\, \mathbf{V}_R \,|\, \mathbf{V}_R \tag{7}$$

with C_D determined by

$$C_D = \begin{cases} 24(1 + 0.15\,\mathrm{Re}^{0.687})/\mathrm{Re} & \mathrm{Re} \le 1000 \\ 0.440 & \mathrm{Re} > 1000 \end{cases} \tag{8}$$

where d is the particle diameter, $\mathbf{V}_R$ the slip velocity between the two phases, and Reynolds number $\mathrm{Re}=|\,\mathbf{V}_R\,|\,d/\nu$.

The gravity and the buoyancy force can be calculated as

$$\mathbf{F}_g = \frac{\pi}{6}d^3(\rho_s - \rho)\mathbf{g} \tag{9}$$

The force due to pressure gradient is

$$\mathbf{F}_p = -\frac{\pi}{4}d^3\nabla p \tag{10}$$

And the added mass force is

$$\mathbf{F}_A = \frac{\pi}{12}d^3\rho\frac{\mathrm{d}\mathbf{u}_s}{\mathrm{d}t} \tag{11}$$

Farrell (Farrell *et al.*, 2004; Farrell *et al.*, 2006) paid close attention to electrostatic field and implied that electrostatic force should also be considered. However, mechanism and quantitative evaluation of static electricity in dust devils is obscure, and the number of

particles which can be tracked at the same time is limited, electrostatic force isn't taken into consideration. The major external forces considered in the present study are enough to represent basic characteristics of dust movement in dust devil.

Implementation

The simulation domain is a cylinder with 1200 m in height, 400 m in diameter, which contains the column of dust devil and the nearby region as illustrated in the bold dashed-lined rectangular region in Fig. 2. In the vertical direction, the vertical grid size is smoothly stretched with the first grid 0.1 m above the surface. The local grid refinement is also applied in the center of dust devil in the horizontal directions to ensure that the detailed structure of dust devil can be obtained. Spatial and temporal discretization employs common second-order schemes.

Dust-devil scale simulation is quite different from the CBL scale simulation. The latter includes the whole region shown in Fig. 2, aiming to reveal the emergence, development and attenuation of thermal convection. The dust-devil scale simulation, however, concerns the dust-devil column in a single thermal cell in the near ground region. Therefore, the initial and boundary conditions of dust-devil scale LES were set according to the background field of the thermal plume in CBL (Gu *et al.*, 2006). The initial radial and vertical velocities are set to zero. The initial temperature below 800 m was 313K, and the region above 800 m was preset as the inversion layer to buffer the violent updraft as many CBL scale simulations did. The surface temperature was 343K to represent typical effect of solar heating on the ground in hot summer afternoons. The ground and the upper boundaries were no slip boundaries. The lateral face was pressure inlet boundary (Zhao *et al.*, 2004). Twenty thousand dust particles were released at the surface in the mature stage. Restricted by the computing capability, the number of released particles was smaller than reality, and particle collision was negligible. Nevertheless, the released particles were enough to show characteristics of dust movement. The true density of dust is 2,600 kg/m^3. A large amount of dust particles with different sizes, 40, 100, 160, and 300 μm, were simulated and tracked in order to give the general shape of dust devil, and to compare trajectories and velocity of particles. According to Table 1 and Table 2, diameters of most loess dusts are less than 30 μm. Therefore, dust particles with a diameter of 40 μm can represent most loess dusts. Large sand particle typically has a diameter of over 200 μm, and particles with a diameter of 300 μm can also be adopted to represent large sand particles. So in the present study, particles with these 4 different sizes can show the overall behaviors of dust devils.

RESULTS AND DISCUSSIONS

When the air flow reaches the mature stage, air strongly spirals up in the core of the thermal plume. The three-dimensional vortex structure results in a low pressure region in the center of the dust devil, especially in the near-surface region of the center. Fig. 3 shows the pressure

Table 1. Main chemical components of Loess dust.

Chemical Component	Content (%)
SiO_2	54~72
Al_2O_3	14~10
Fe_2O_3	5~0.3
CaO	9~4

Table 2. Diameter distribution of Loess dust.

Diameter (μm)	Content (%)
0~5	32±3
5~10	21±3
10~20	24±4
20~30	12±2
>30	11±5

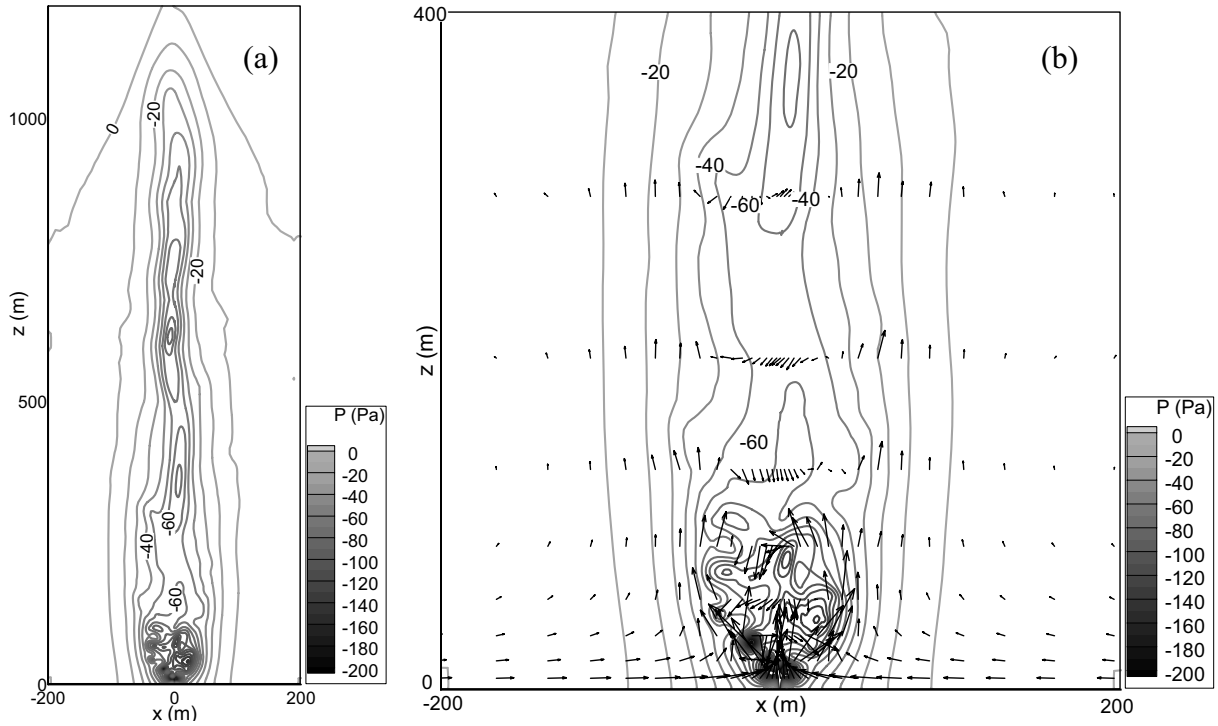

Figs. 3. Profiles of pressure drop contours. (a) The whole computation domain. (b) The enlarged near-surface region (400 × 400 m) together with radial-vertical velocity vector.

drop in the $y = 0$ slice. The maximum pressure drop is over 2 hPa in the near-surface region of the core. Pressure drop in the core is obviously larger than in the outer region, and this provides centripetal force to maintain horizontal rotation. The radial-vertical velocity vector in the enlarged near-surface region (Fig. 3b) indicates that air flows toward the center of the

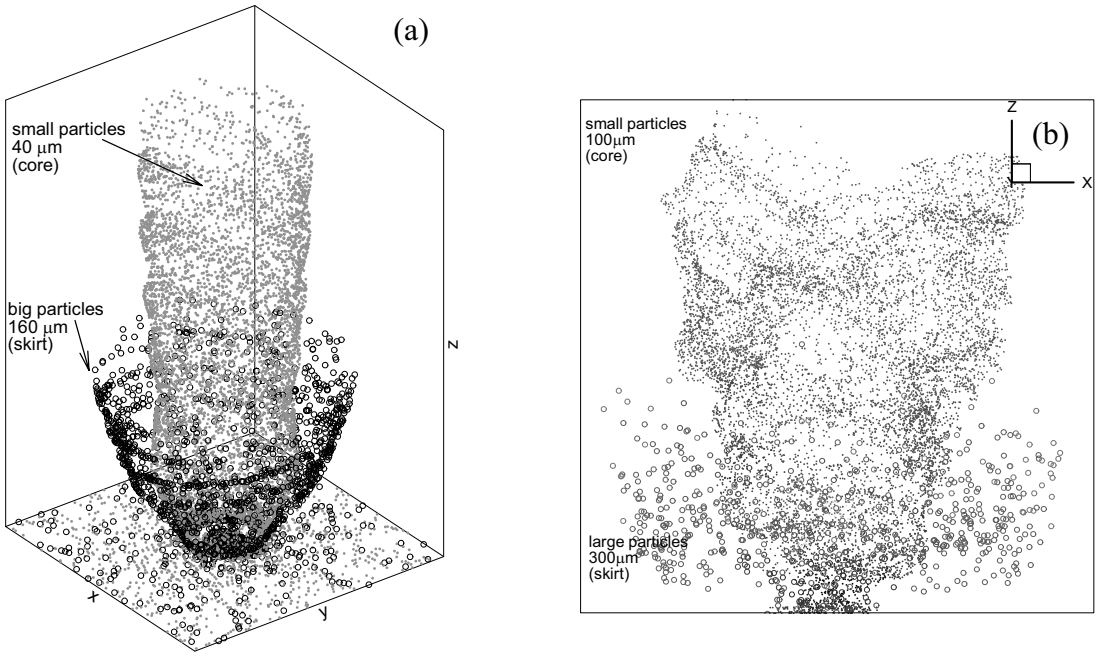

Figs. 4. Spatial distributions of dust particles in the central region (30 × 30 × 40 m), (a) comparison of 40 μm and 160 μm particles; (b) comparison of 100 μm and 300 μm particles (small particles are denoted with dots, big particles with hollow big circles).

whirlwind in the near-surface region and turns upward in the lower part of the whirlwind. The air updraft can reach 15 m/s in the region with large pressure drop. The weak downdraft in the upper central part of the dust devil forms the whirlwind eye and also impedes the spread of dust particles. The present numerical results of pressure drop and velocity vector in the whirlwind correspond well with observations (Ives, 1947; Hall, 1981; Hess and Spillane, 1990).

Dust devil, as an aeolian transport system, has been studied by Metzger (1999). Gu *et al.* (2006) gave more detailed picture of dust devil to study the dust lifting mechanism. By means of calculating the forces exerted on lots of individual dust particles and therefore their velocities, the movement of particles in whirlwind and the overall shape of dust devil can be simulated by Euler-Lagrange approach.

Fig. 4 shows spatial distributions of dust particles with different diameter in the simulated dust devil. Fig. 4a compares spatial distribution of 40 μm and 160 μm particles in three-dimensional view, and Fig. 4b compares spatial distribution of 100 μm and 300 μm particles in *x*-*z* plane. Only particles lying in the center of the ground (the region with significant air updraft in whirlwind) can be lifted. In Fig. 4a, 40 μm dusts are lifted and form a cylindrical shape, while 160 μm particles a conical shape. The outward scattering of 160 μm particles isobvious and makes most of 160 μm particles lying out of 40 μm dusts. Similar result can be found in Fig. 4b in which the outward scattering of 300 μm particles makes them look

like a bowl. The difference in elevation height of particles is also shown in Fig. 4. The appearance of the simulated dust devil is quite similar to observed dust devils (Fig. 1). The main column of dust devil contains most of small particles. Large particles are lifted only to a limited height, spread outward and form the "skirt" around the base of the main column. Real shapes of dust devils vary with the whirlwind and properties of dust/sand, but the overall patterns of dust devils are the same as simulated dust devils. The negative vertical pressure gradient in the dust devil helps particle to be lifted, unlike in the horizontal wind systems where the negative vertical pressure gradient isn't a major driving force. Once dusts leave the ground in the dust devil, the revolution of particles is mainly maintained by the pressure gradient force exerted by the air. The centrifugal force makes big particles easy to be thrown outwards, while small dusts can spin up to a height of hundreds of meters.

Fig. 5 gives projections of velocity vectors of 100 μm and 300 μm particles. For clarity, 300 μm particles in the front half of the computational domain, $y < 0$, are drawn, while 100 μm particles in the back half are drawn. Vectors are drawn every 20 particles. Fig. 5a is *x-z* projection for 100 μm particles in the back half region; Fig. 5b is *x-z* projection for 300 μm particles in the front half region; and Fig. 5c is *x-y* projection for both 100 μm and 300 μm particles. Both the direction and relative magnitude of velocity vector reveal properties of particle movements. Most particles with high speed locate at the central near-surface region. Small dusts (100 μm) can be lifted to over 30 m in height and still maintain positive vertical velocity. Large sand grains (300 μm), however, can be lifted to about 15 m high only. Vertical speeds of many large grains are quite low. And large grains, which are thrown out of the main body of whirlwind, drop down to the ground gradually.

Instantaneous statistics of 100 μm and 300 μm particles distributions in the vertical direction are shown in Fig. 6. Percentage of the number of particles every 1 m in the vertical direction is given in Fig. 6a. The vertical percentage distribution of 100 μm particles is smoother than that of 300 μm particles. Percentage of 300 μm particles increases with height rapidly below 5 m, and then decreases over the height of 5 m. The maximum percentage of 300 μm particles at a height of 5 m indicates that it's not easy to move large particles to a long distance. Fig. 6b gives the mean vertical speed computed by the following expression

$$W_m = \frac{1}{n}\sum_{i=1}^{n} w_i \tag{12}$$

where W_m is the mean vertical speed, w_i the vertical speed of *i*-indexed particle, n the number of particles located at heights ranging from x-1 to x m (x = 1, 2, …, 30) . Similar to Fig. 6b, Fig. 6c gives the mean elevation angle of velocity vector, with elevation angle defined as

$$\theta_i = \arcsin\left(\frac{w_i}{\sqrt{u_i u_i + v_i v_i + w_i w_i}}\right) \tag{13}$$

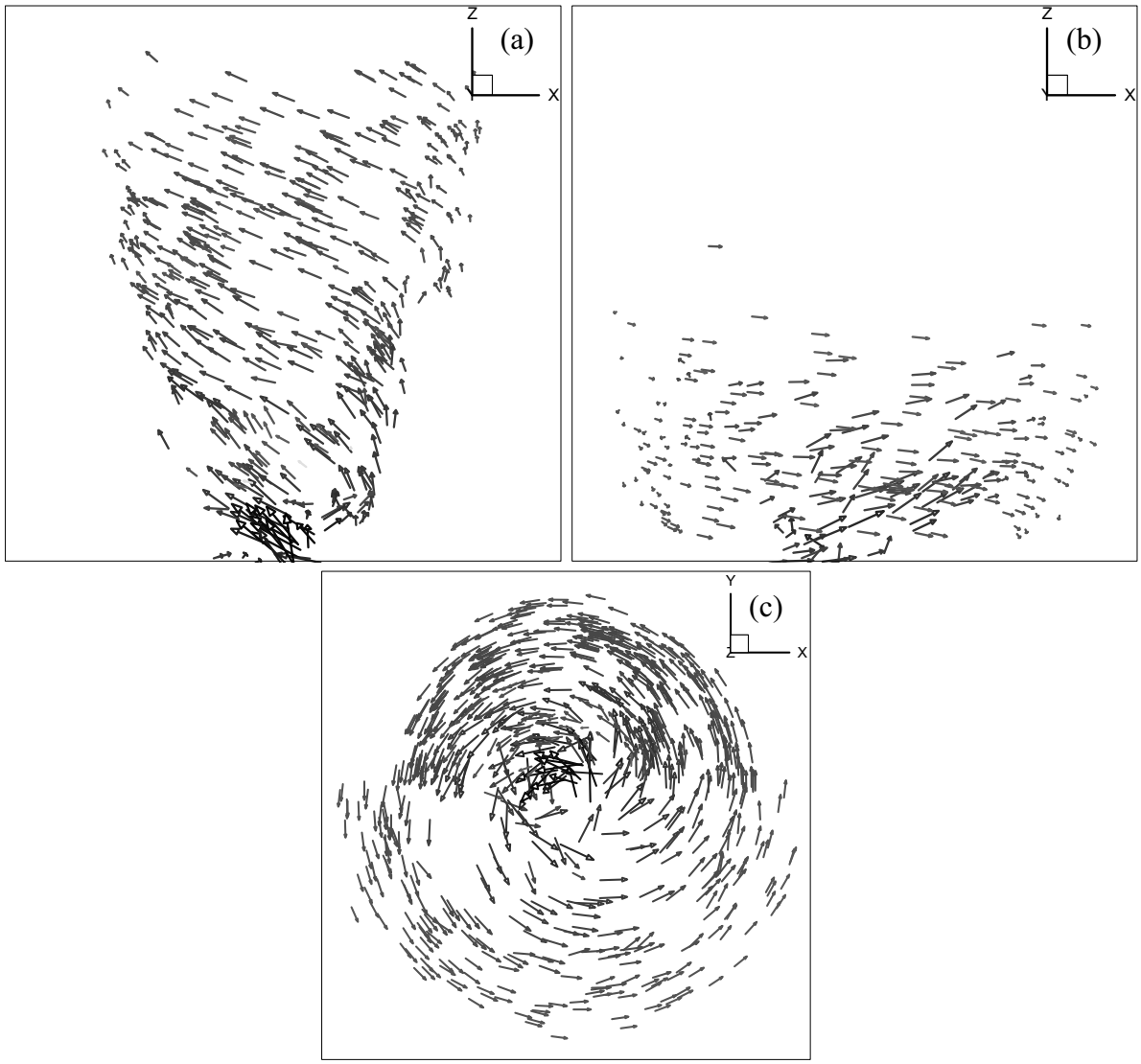

Figs. 5. Velocity vectors of 100 μm and 300 μm particles in the central 30 × 30 × 40 m region, (a) *x-z* projection for 100 μm particles, (b) *x-z* projection for 300 μm particles, (c) *x-y* projection for both 100 μm and 300 μm particles. For clarity, 300 μm particles in the front half of the domain, $y < 0$, are drawn, and 100 μm particles in the back half, $y > 0$, are drawn.

The maximum mean vertical speed and mean elevation angle of 300 μm particles occur just above the ground. When 300 μm particles move to a height over 3-5 m, mean vertical speed and mean elevation angles are close to zero, and the emergence of small negative value indicates the decline of large particles.

On the other hand, 100 μm small particles maintain positive mean vertical speed and mean elevation angle in the whole 30 m above the ground. Maximum mean vertical speed of 100 μm particles locates at about 2 m above the ground, while maximum mean elevation angle locates at about 8 m above the ground. Variations of statistics of 100 μm particles are moderate in the region above 10 m, where 300 μm large particles are sparse. Mean elevation angle distribution of 300 μm particles (Fig. 6c)

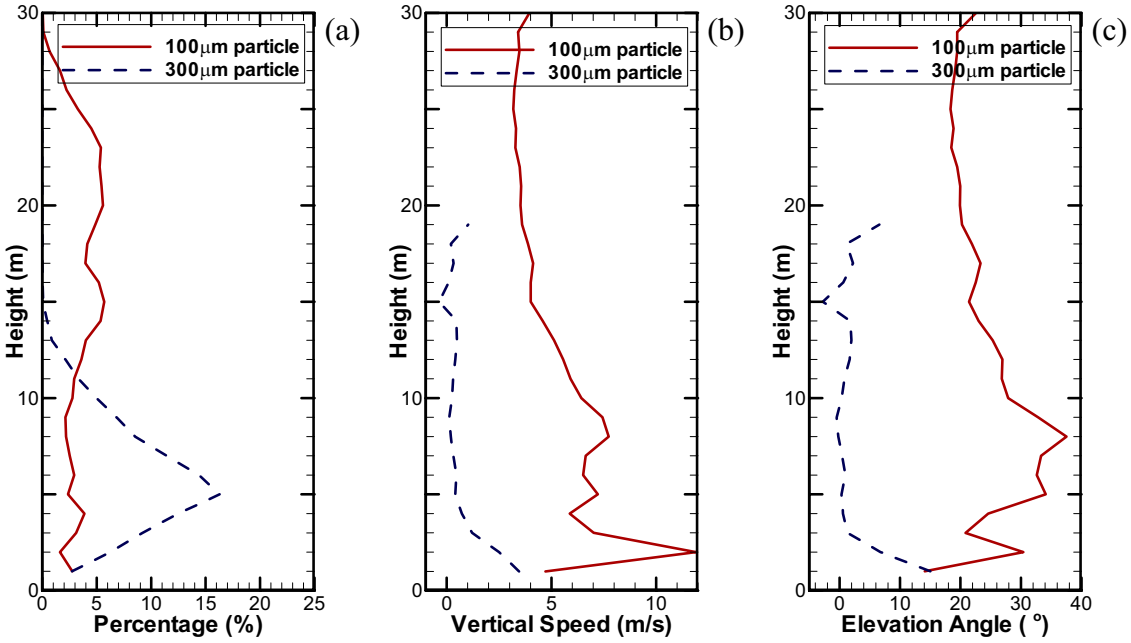

Figs. 6. Comparisons of statistics of 100 μm and 300 μm particles, (a) percentage of number of particles, (b) mean vertical speed, (c) mean elevation angle of velocity vector.

shows that 300 μm large particles have reached their maximum elevation height, 15 m (Fig. 6a). Owning to the short integral time, 100 μm particles at the highest altitude still have positive elevation angle, which means that the simulated dust devil can raise small particles much higher than 30 m if the simulation continued.

According to the simulation results of dust devil, trajectories of particles with different diameters in dust devils, as shown in Fig. 7, cannot be perfectly described by the common mechanism of horizontal wind shear transport system. In the simulated whirlwind system, particles with diameter smaller than 40 μm can spiral up in the cylindrical shape illustrated as the curve (a) in Fig. 7, and form the major visible part of dust devil. Particles with a diameter close to 100 μm are lifted in the conical shape with small cone angle illustrated as the curve (b) in Fig. 7. The curves (c) and (d) represent dust-lifting patterns for 160 μm and 300 μm particles, respectively.

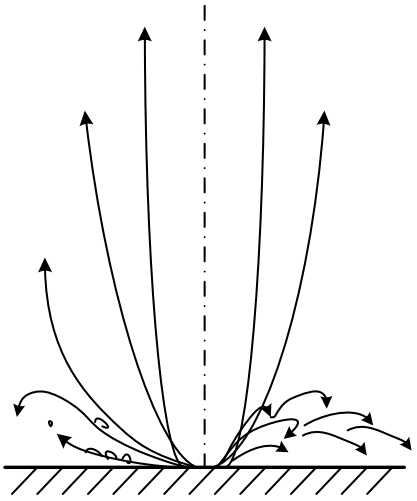

Fig. 7. Sketch of dust-lifting patterns in dust devil.

Large particles are thrown out of the whirlwind and then fall to the ground. They

often form the outer skirt around the base of dust devil. The strength of the whirlwind can influence its dust-lifting capability. Nevertheless, these typical simulated dust-lifting patterns remain and conform to reality. The whirlwind with a low-pressure heat core makes dusts lifted easily from the ground, as compared with horizontal wind system. Dust devils often occur in the convective boundary layer with small mean horizontal wind speed. Since thermal plumes are the basic property of CBL, there are many potential spots where dust devil can take place. Although the total contribution of dust devils to floating dusts is difficult to evaluate till now, it's believed that dust devil is an important way to lift dusts into the air.

Loess Plateau is the largest loess deposition zone in the world. Mean diameter of loess dust is small. Basic properties of loess dust are given in Table 1 and Table 2. More than 90% loess dusts are smaller than 40 μm in diameter. According to the present simulation results, most loess dusts can be easily lifted to a high altitude through dust devils. These small loess dusts can be suspended and diffuse in the air for a long period, and have been proved as the major source of PM_{10} and TSP. The phenomenon that the concentration of TSP exceeds the standard value in most of days on the Loess Plateau is a result of natural circumstances. Dust devil provides a key channel to transport dusts from the ground to the air in convective boundary layer. Because loess dusts are small and easy to be lifted and dust devils can occur frequently in CBL, especially in direct sunlight, dust devil plays an important role in the formation of the background PM_{10} (including TSP) on the Loess Plateau.

SUMMARY

Dust devil in the convective boundary layer is simulated by Euler-Lagrange approach. By means of large-eddy simulation method, smoothly stretched grid and carefully set boundary conditions in the specific circumstances, flow fields of the small scale whirlwind are obtained. Movements of 20,000 dust particles are tracked by computing external forces and velocities with the aid of simulated high-resolution air flow fields. Dust-devil-scale numerical simulation of this gas-particle two-phase flow gives an insight into the appearance and nature of dust devils.

Characteristics of the simulated airflow are in good accordance with field observations. Statistics of particle trajectories give striking shapes of dust devils. Small particles with diameter of 0.04 mm can be lifted easily to a high level and form a rolling cylinder. 0.1 mm dust particles spiral upwards like a cone with a small cone angle. Both 0.16 mm and 0.3 mm particles are obviously thrown outward with limited elevation height and fall back to the ground. By virtue of figures of the three-dimensional velocity vector of dust particles, it is revealed that a wide range (< 0.3 mm) of dust particles can be lifted at the surface-atmosphere interface by the small whirlwind.

Numerical results explain why TSP/PM_{10} concentration exceeds the Standard greatly all

the year round on the Loess Plateau, where the loess dust coming from the local surface is the major source of TSP. 90% loess dusts are smaller than 0.04 mm in diameter, which makes them lifted easily to a certain height by dust devils even without obvious mean horizontal wind. Because the thermal plumes, which can lead to whirlwinds and thereafter dust devils, are common in CBL, dust devils come into being frequently in multi-locations of the Loess Plateau, especially in direct sunlight. According to the nature circumstances of the Loess Plateau and the thermodynamic characteristics of dust devil, the dust-devil-scale simulation indicates one source of the background TSP/PM_{10} on the Loess Plateau and how they are lifted into the atmosphere.

ACKNOWLEDGEMENTS

The project is financially supported by the National Natural Science Foundation of China (No. 40675011), and the National Basic Research Program of China (No. 2004CB720208). The authors also appreciate the support of Key Laboratory of Mechanics on Western Disaster and Environment.

REFERENCES

Fan, L.S. and Zhu, C. (1998). *Principles of Gas-solid Flows.* Cambridge Univ. Press.

Farrell, W.M., Renno, N. and Delory, G.T. (2006). Integration of Electrostatic and Fluid Dynamics within a Dust Devil. *J. Geophys. Res.* 111(E1): Art. No. E01006.

Farrell, W.M., Smith, P.H. and Delory, G.T. (2004). Electric and Magnetic Signatures of Dust Devils from the 2000-2001 MATADOR Desert Tests. *J. Geophys. Res.* 109(E3): Art. No. E03004.

Germano, M., Piomelli, U., Moin, P. and Cabot, W.H. (1991). A Dynamic Subgrid-scale Eddy Viscosity Model. *Phys. Fluids.* A3: 1760-1765.

Gierasch, P.J. and Goody, R.M. (1973). A Model of a Martian Great Dust Storm. *J. Atmos. Sci.* 30: 169-178.

Greeley, R., Balme, M.R., Iversen, J.D., Metzger, S., Mickelson, R., Phoreman, J. and White, B. (2003). Martian Dust Devils: Laboratory Simulations of Particle Threshold. *J. Geophys. Res.* 108(E5): Art. No. 5041.

Gu, Z.L., Zhao, Y.Z., Li, Y., Yu, Y.Z. and Feng, X. (2006). Numerical Simulation of Dust Lifting within Dust Devils-Simulation of an Intense Vortex. *J. Atmos. Sci.* 63: 2630-2641.

Hall, F.F. (1981). Visibility Reductions from Soil Dust in the Western United States. *Atmos. Env.* 15: 1929-1933.

Hess, G.D. and Spillane, K.T. (1990). Characteristics of Dust Devils in Australia. *J. Appl. Meteor.* 29: 498-507.

Ives, R.L. (1947). Behavior of Dust Devils. *Am. Met. Soc. Bull.* 28: 168-174.

Kanak, K.M., Lilly, D.K. and Snow, J.T. (2000). The Formation of Vertical Vortices in the Convective Boundary Layer. *Quart. J. Roy. Meteor. Soc.* 126: 2789-2810.

Leovy, C.B. (2003). The Devil Is in the Dust. Nature 424: 1008-1009.

Metzger, S.M. (1999). *Dust Devils as Aeolian Transport Mechanisms in Southern Nevada and in the Mars Pathfinder Landing Site.*

Ph.D. thesis, Univ. of Nev.

Renno, N.O., Burkett, M.L. and Larkin, M.P. (1998). A Simple Thermodynamical Theory for Dust Devils. *J. Atmos. Sci.* 55: 3244-3252.

Sinclair, P.C. (1973). The Lower Structure of Dust Devils. *J. Atmos. Sci.* 30: 1599-1619.

Smith, R.K. and Leslie, L.M. (1976). Thermally Driven Vortices: a Numerical Study with Application to Dust-devil Dynamics. *Quart. J. Roy. Meteor. Soc.* 102: 791-804.

Toigo, A.D. (2003). Numerical Simulation of Martian Dust Devils. *J. Geophys. Res.* 108(E6): Art. No. 5047.

Xu, X.D., Zhou, M.Y. and Chen, J.Y. (2002). A Comprehensive Physical Pattern of Land-air Dynamic and Thermal Structure on the Qinghai-Xizang Plateau. *Sci. China Ser. D.* 45: 577-594.

Zhao, Y.Z., Gu, Z.L., Yu, Y.Z., Ge, Y., Li, Y. and Feng, X. (2004). Mechanism and Large Eddy Simulation of Dust Devils. *Atmos.-Ocean* 42: 61-84.

Received for review, March 31, 2007

Accepted, November 15, 2007